Engineering Structures 117 (2016) 118–129

Contents lists available at ScienceDirect

Engineering Structures

journal homepage: www.elsevier.com/locate/engstruct

A finite element study of the effect of vertical loading on the in-plane behavior of concrete masonry infills bounded by steel frames

Xi Chen, Yi Liu *

Dept. of Civil and Resource Engineering, Dalhousie Univ., Halifax, NS B3J 1Z1, Canada

ARTICLE INFO

Article history:
Received 30 November 2015
Revised 2 March 2016
Accepted 3 March 2016
Available online 21 March 2016

Keywords:
Concrete masonry infills
In-plane behavior
Stiffness and strength
Combined vertical load and lateral load
Finite element
Analytical model

ABSTRACT

A finite element study was performed to investigate the effect of vertical loading on the in-plane lateral behavior and strength of concrete masonry infills bounded by steel frames. An experimental program was also conducted and results were used to verify the finite element model. Parameters considered in the finite element study included the vertical load level and application method, infill aspect ratio, infill compressive strength, and bounding frame stiffness. Results showed that when applied as a uniformly distributed load on the frame beam, an optimal load level was identified and the vertical load, when applied within this load level, was found to be beneficial to the lateral stiffness and strength of the infilled frame. When applied as point loads on columns, the vertical load was shown to reduce the lateral strength of the infilled frame. Based on the regression analysis on finite element results, a simplified analytical model was proposed to account for the effect of vertical loading through the use of a modification factor on the lateral stiffness and strength of infilled steel frames. The proposed model was shown to provide results in good agreement with finite element values over a wide range of load levels, infill material strengths, and frame stiffnesses.

1. Introduction

Behavior and capacity of masonry infills built inside concrete or steel frames have been given increasing research attention in recent years. It is widely accepted that when the infill is built in tight contact with the bounding frame with an intention to participate in the load sharing, its inherently large in-plane stiffness will attract additional forces to the frame area and change the behavior of the frame system. If not designed properly, the structural integrity of both the infill and frame will be compromised. It is thus crucial to accurately evaluate the contribution of the infill to the stiffness and strength of the frame system. To that end, considerable amount of experimental research has been conducted with majority being around 1980's to 2000's ([1–8]). With the development of computer technology in the past two decades, numerical studies using computer codified finite element methods have been shown to be an effective tool in research on masonry infills ([9–15]). In finite element modeling, macro- and micro-modeling techniques are two often employed categories of techniques. The "diagonal strut" concept is one of the commonly used macro-modeling methods, where the infill is replaced by an equivalent diagonal strut acting in compression to resist the lateral loading. Once the strut width is known, a simple frame analysis can be performed to determine the stiffness of the system. The strength of the infill can also be related to the diagonal strut width. Several analytical equations on the diagonal strut width have been proposed by various researchers ([16–21]). However, several studies ([22–27]) also showed that single-strut models were inadequate for capturing the force and moment in the members of the bounding frame and various multi-strut models were then proposed to overcome such limitations. Regardless of single or multi-strut approach, proposed equations were calibrated using experimental results to a specific set of testing parameters and thus none was found to provide universally satisfactory estimate for infilled systems with different infill and frame material and geometric properties. In the case of micro-modeling, a smeared-crack continuum was often used to model masonry infills. The mortar effect was accounted for using various interface models where different failure surfaces can be implemented to simulate shear and tension failure at mortar joints. Al-Chaar and Mehrabi [28] showed that a combination of the smeared-crack continuum formulation developed by Lotfi and Shing [29] and the interface model developed by Mehrabi and Shing [30] can be used for numerical study of infilled reinforced concrete (RC) frames. In the finite element study conducted by Stavridis [31], masonry infills were modeled as rectangular

* Corresponding author. Tel.: +1 (902) 494 1509; fax: +1 (902) 494 3108.
E-mail address: yi.liu@dal.ca (Y. Liu).

http://dx.doi.org/10.1016/j.engstruct.2016.03.010
0141-0296/

smear-crack continuum elements that were inter-connected with zero-thickness interface elements with cohesive crack formulation developed by Lotfi and Shing [32]. In both cases, the model was shown to have the capability of predicting lateral load-carrying capacity and failure mechanisms of RC infilled frames.

Noting that all above mentioned research was conducted on infilled frames subjected to in-plane lateral loading only, this paper focused on the investigation of vertical load effect on the lateral stiffness and strength of the infilled frames. The presence of vertical loading on the bounding beam or columns could be a common occurrence in practice. If the bounding frame is an integral part of the gravity loading system, the vertical load can be either applied through columns or beams depending on the framing plan. Fiorato et al. [33], Mehrabi et al. [30], Manos et al. [34], and Stylianidis [35] conducted experimental tests on masonry infilled RC frames under lateral load along with vertical load applied on the frame columns. Test results showed that the vertical load applied on the frame columns resulted in an increase in the lateral stiffness and strength of the infilled system. Papia et al. [36] developed an analytical method where the vertical load effect can be accounted for by multiplying a factor (k) to the diagonal strut width obtained for infills subjected to lateral load only. Based on finite element results obtained by Cavaleri et al. [37], Amato et al. [38] and Campione et al. [39] derived the k factors for square infills and rectangular infills respectively to account for the presence of vertical loads applied at the beam–column joints. Asteris [40] integrated the work of Papia et al. [36] and Amato et al. [38] and proposed an analytical equation taking into account the effect of both the opening in the infill wall and the vertical load applied at the beam–column joints as well as the interaction between the two. The aforementioned studies were all on masonry infilled RC frames where the k factors in these studies were developed for determination of only the initial stiffness of the infilled systems. Comparing to infilled RC frames, the research on infilled steel frames was limited in the available literature. One such study was conducted by Stafford-Smith [41] nearly 50 years ago where infills made of just mortar and bounded by steel bar frames were tested under a lateral load and a uniformly distributed vertical load imposed on the upper beam of the frame. The study found that vertical load up to a certain level increased the lateral stiffness and strength of the infill. However, no quantified correlation between the vertical load and the lateral stiffness and strength was provided. Due to different characteristics between RC and steel frames, it is believed that extent of interaction between the infill and its bounding frame is affected by the material of frames (eg. steel or RC). The results obtained for RC bounding frames may not be directly applicable to steel bounding frames. Hence, a finite element study was motivated to investigate the effect of vertical loading on the in-plane behavior and capacity of infills bounded by steel frames. Concurrent with the finite element study, an experimental program was also conducted and the results obtained from this study as well as those from the available literature were used to examine the robustness and efficacy of the finite element model. The main objective of this study was to determine the correlation between the vertical load and the lateral stiffness and strength of the infilled steel frame. The effects of a wide range of geometric and material properties of the infilled frame, vertical load levels as well as manners of application were included in the study.

2. Experimental study

The experimental program was conducted by the same research group at the Dalhousie University [42,43]. Masonry infilled steel frames subjected to either lateral loading or combined lateral and vertical loading were tested. The infill walls with an aspect ratio (height/length) of 1:1.3 were constructed using Type S mortar and custom made one-third scale of standard 200 mm concrete masonry unit (CMU). Partially grouted and fully grouted infills were considered. Three axial load levels including 111 kN, 80 kN, and 49 kN were considered and they represented from 2.8% to 6.4% of the axial capacity of the W100 × 19 column. The test setup is shown in Fig. 1 (a). The steel frame was constructed using W100 × 19 steel section for all members. The steel section was selected according to the design guidelines specified in the Canadian steel design standard CSA S16-14 [44]. The infill was simply positioned inside the steel frame without any mechanical connectors between the infill and the frame. The infilled frame was then supported on a stiffened steel beam which was in turn bolted to the strong floor through closely spaced steel rods as seen in the figure. A hydraulic actuator with a capacity of 250 kN was used to apply lateral load to the failure of the specimen. A skewed A-frame consisting of two steel columns provided a reaction support for the lateral load whereas two leaning columns provided out-of-plane bracing for the reaction column, as shown in Fig. 1(b). In the case of combined lateral and axial loading, the axial load was first applied to the pre-determined level using a hydraulic jack and was kept constant as the lateral load applied till the failure of the specimen. A stiffened W beam was used to distribute the axial load onto the top beam through the two roller assemblies at the two one-third points of the beam.

3. Finite element model

3.1. Model description

The software ANSYS was used in the development of the model. In this study, a simplified micro-modeling technique was used where the infill was modeled using homogeneous continuum elements, and the mortar effect was simulated using a surface-based cohesive contact model to capture the cracking and sliding failure of the mortar joints. A schematic view of the modeled infilled frame is shown in Fig. 2(a). The masonry infill was modeled using a four-node plane stress element, PLANE42, placing in running bond. Each masonry unit was expanded in each directions by the half mortar thickness and the expanded mortar units interact with each other through the interface. The interface was modeled using surface-based cohesive contact pairs. Each contact pair consists of a zero-thickness surface-to-surface cohesive zone interface element, CONTA171, and a zero-thickness target element TARGE169. The CONTA171 element was used to detect contact or separation between "target" surfaces (TARGE169) and a deformable surface defined by the CONTA171 element. This interface element was also used for the contact between the infill and the frame members. The geometry and configuration of inter-blocks contact pairs are shown in Fig. 2(b).

3.2. Material model and failure criteria

An elastic perfect plastic material model was used for frame members where the elastic modulus and the yield strength of steel were taken as 200 GPa and 350 MPa, respectively. The constitutive model for masonry adopted the one proposed by Priestley and Elder [45] which was calibrated with experimental results and it is expressed in Eq. (1). It should be pointed out that this model was assumed homogenous.

$$\varepsilon \leqslant 0.0015, \quad \sigma = \frac{f'_m}{0.9375}\left(\frac{2\varepsilon}{0.002} - \left(\frac{\varepsilon}{0.002}\right)^2\right) \tag{1a}$$

$$0.0015 \leqslant \varepsilon \leqslant 0.0025, \quad \sigma = f'_m(1 - z_m(\varepsilon - 0.0015)) \tag{1b}$$

$$\text{where} \quad z_m = \frac{0.5}{\frac{3+0.29f'_m}{145f'_m - 1000} - 0.002} \tag{1c}$$

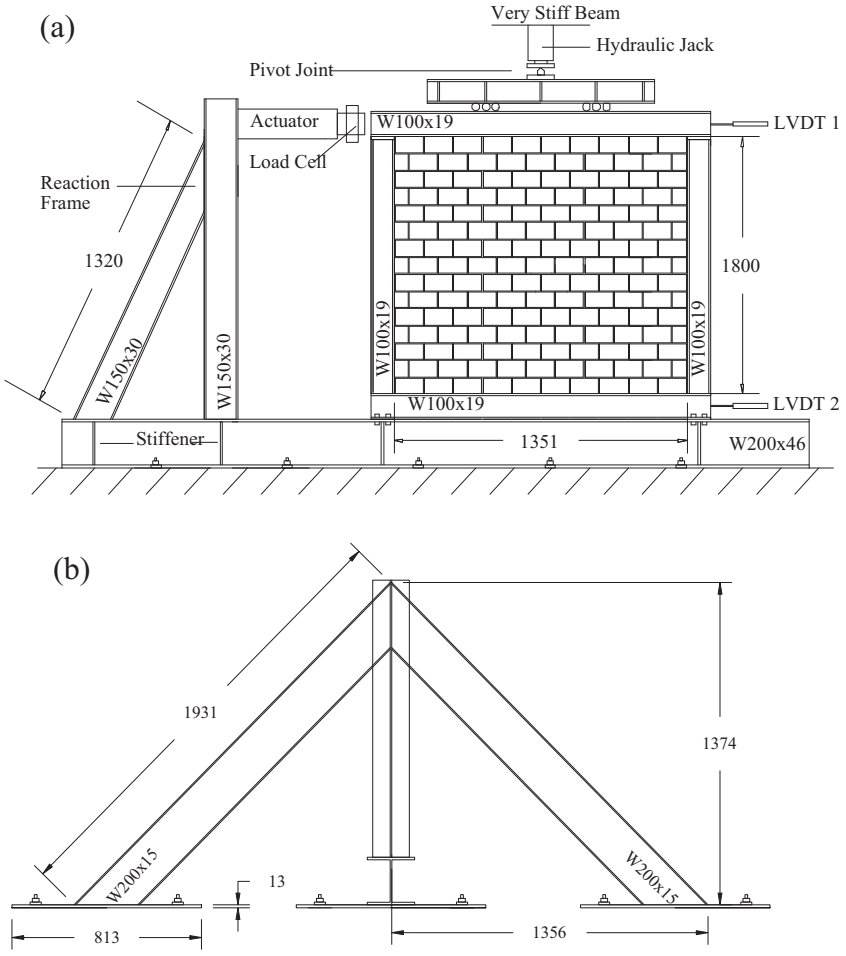

Fig. 1. Test setup, dimensions in mm: (a) schematic view; and (b) out-of-plane bracing for the loading column.

Cracking and sliding failure of mortar joints were monitored using the linear elastic traction–separation laws as shown in Fig. 3. Represented by the bilinear cohesive zone material model of the CONTA171 element, separation initiates when the maximum normal or shear stress in a contact pair reaches the corresponding strength. The shear stress and the relative slip behavior is plotted in Fig. 3(a) which shows separation begins at point A where the shear strength (τ_t) is achieved and is completed at point C when the shear stress reaches zero. The softening stage provides mortar joints with a residual shear strength to account for the frictional resistance of the joint after shear crack occurred. For tension separation, a similar bilinear constitutive relationship but with a cut-off was adopted. As Fig. 3(b) shows, once the tension stress in the contact pair reaches the tensile strength (f_t) of mortar joint, the contact pair is considered separated to represent the tensile cracking of mortar joint. The values of the normal and shear stiffness were determined based on the following expressions suggested by Lourenço [46]:

$$k_n = \frac{E_u E_{mor}}{t_m(E_u - E_{mor})} \tag{3}$$

$$k_s = \frac{G_u G_{mor}}{t_m(G_u - G_{mor})} \tag{4}$$

where E_u and E_{mor}, and G_u and G_{mor} are the Young's moduli and shear moduli of masonry unit and mortar respectively; and t_m is the thickness of mortar joints. In lieu of experimental data, G_u and G_{mor} can be taken as $0.4E_u$ and $0.4E_{mor}$ respectively.

The damage initiation criterion is defined using a Mohr–Coulomb friction yield surface combined with a tension cut-off and elliptical compression cap as shown in Fig. 4 where f_t is the tensile strength of mortar joint and φ is the friction angle. Note that the compression cap was defined using a Hill type yield criterion proposed by Lourenço and Rots [47] to monitor the compression failure of masonry infill. This failure surface has been shown by Lourenço [46] and Al-Chaar and Mehrabi [28] to produce reasonably accurate estimates when compared with experimental results.

3.3. Boundary conditions and loading procedure

The frame beam-to-column connection was modeled as rigid and the columns were assumed to be fix-supported at ends. A monotonically increased load with a defined load increment was applied at the frame beam level. During each increment of loading, the stress was determined for each element based on its assigned constitutive model. The tensile and shear failure were checked at the interface and the compression failure was checked at each masonry unit based on the failure surface defined above. If failure was detected, the tangent stiffness of the element associated with the failure at that load increment was modified according to the material constitutive model described above; and the analysis was rerun with the updated system stiffness matrix until no new failure was detected. The entire process was repeated for the subsequent increment of load. To obtain the falling branch in the load vs. lateral displacement response, an augmented spring was implemented as shown in Fig. 2(a). In a load controlled analysis, the infill

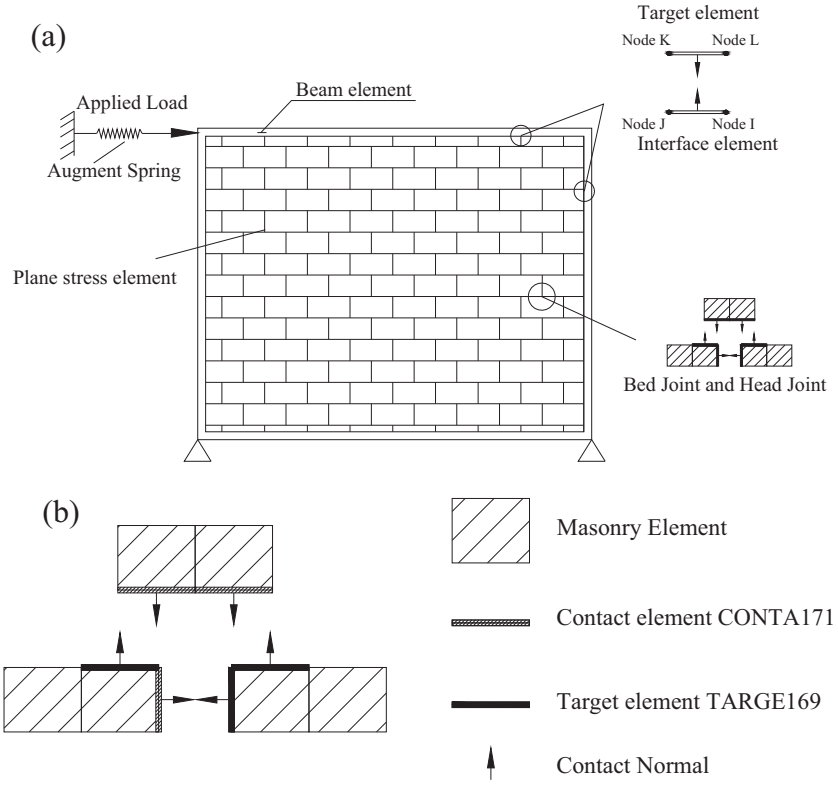

Fig. 2. (a) Finite element model of the infilled frame, and (b) configuration of a joint.

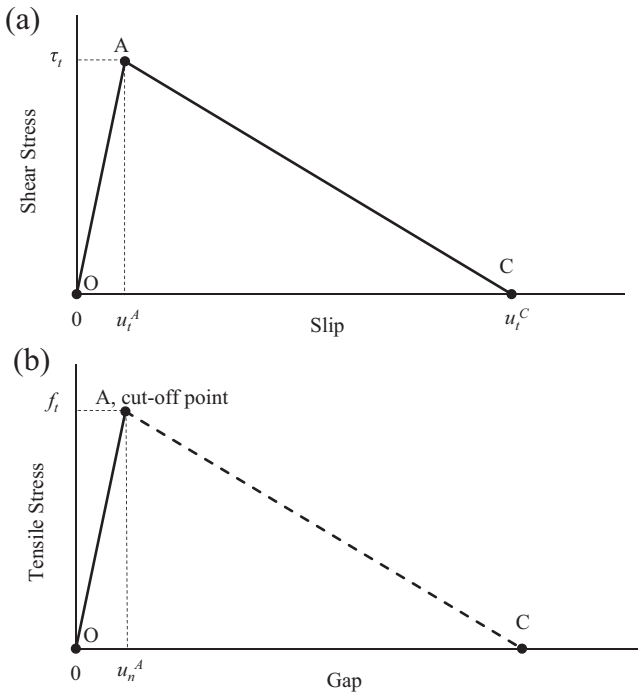

Fig. 3. Constitutive relationship for cohesive material, (a) shear stress vs slip, and (b) normal stress vs gap.

cracking and crushing could lead to a sudden loss of infill stiffness which may in turn result in convergence problem. The spring was then implemented to regulate the load when the infill suddenly cracked or crushed so that the load vs. lateral displacement curve can reflect this load drop. The stiffness of this spring was set to be equal to the initial stiffness of the infilled frame.

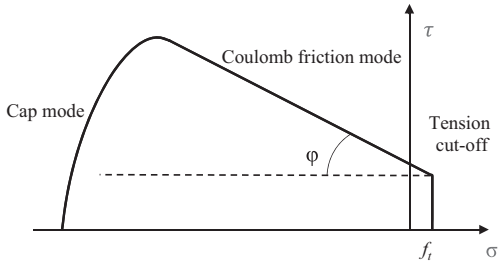

Fig. 4. Mohr–Coulomb friction yield surface.

3.4. Verification of the finite model

The finite element (FE) model was validated using experimental results obtained from this research [42] on infilled frames subjected to combined vertical and lateral loading. To demonstrate the robustness of the model, it was also validated using results reported in the available literature ([1–3]). Steel frames infilled with concrete masonry panels and loaded statically or quasi-statically were used in the validation. Twenty specimens were considered, of which 14 were subjected to lateral load only and six were subjected to combined lateral and vertical load. Detailed descriptions of specimens are presented in Table 1. Table 2 summarizes the comparison results where k_{exp} and P_{exp} are the experimental crack stiffness and ultimate load whereas k_{FE} and P_{FE} are the corresponding finite element results. Table 2 shows that for infills subjected to either lateral load only or combined loading, the average test-to-FE ratios of ultimate load and stiffness are all close to unity with overall coefficient of variation (COV) of 14% for crack stiffness and 7% for ultimate load. This suggests that the finite element model is accurate in providing the stiffness and strength estimates and this accuracy is reasonably consistent for

Table 1
Detail description of the experimental specimens.

		H (m)	L (m)	f'_m (MPa)	E_m (MPa)	t_e (mm)	Beam section	Column section	Vertical load (kN)
		Infills subjected to combined loading							
Liu and Manesh [42]	CF-1	1.08	1.35	9.1	12,800	64	W100 × 19	W100 × 19	111
	CF-2	1.08	1.35	9.1	12,800	64			80
	CF-3	1.08	1.35	9.1	12,800	64			49
	CP-1	1.08	1.35	9.4	10,100	43			111
	CP-2	1.08	1.35	9.4	10,100	43			80
	CP-3	1.08	1.35	9.4	10,100	43			49
		Infills subjected to lateral load only							
McBride [1]	WA1	2.8	3.6	27.4	23,290	66	W250 × 58	W200 × 46	
	WA2	2.8	3.6	27.7	23,545	66			
	WA3	2.8	3.6	26.5	22,525	66			
	WA4	2.8	3.6	24.4	20,740	66			
Yong [2]	WB1	2.8	3.6	23.7	20,145[a]	66	W250 × 58	W200 × 46	
	WB2	2.8	3.6	33.3	28,305[a]	66			
	WB3	2.8	3.6	31.4	26,690[a]	66			
Amos [3]	WC1	2.8	3.6	31.7	26,945[a]	66	W250 × 58	W200 × 46	
	WC2	2.8	3.6	27.7	23,545[a]	66			
	WC7	2.8	3.6	33.4	28,390[a]	66			
Liu and Soon [43]	P1NA	1.08	1.08	8.6	10,496	43	W100 × 19	W100 × 19	
	F1NA	1.08	1.08	9.6	14,430	64			
	P3NA	1.08	1.35	7.3	10,496	43			
	F3NA	1.08	1.35	10.3	14,430	64			

[a] E_m was not reported in the paper, a value of $850f'_m$ was assumed.

Table 2
Stiffness and strength comparison of the experimental and FE results.

		k_{exp}	P_{exp}	k_{FE}	P_{FE}	$\frac{k_{exp}}{k_{FE}}$	$\frac{P_{exp}}{P_{FE}}$
		Infills subjected to combined loading					
Liu and Manesh [42]	CF-1	37	198	36	203	1.03	0.98
	CF-2	32	169	32	163	1.00	1.04
	CF-3	29	152	28	161	1.04	0.94
	CP-1	26	126	28	133	0.93	0.95
	CP-2	25	120	27	129	0.93	0.93
	CP-3	26	109	24	99	1.08	1.10
Avg						1.00	0.99
C.O.V (%)						6	7
		Infills subjected to lateral load only					
McBride [1]	WA1	73	471	68	475	1.07	0.99
	WA2	82	440	90	420	0.91	1.05
	WA3	74	463	87	455	0.85	1.02
	WA4	63	476	77	449	0.82	1.06
Yong [2]	WB1	72	449	80	409	0.90	1.10
	WB2	74	538	81	581	0.91	0.93
	WB3	74	556	80	549	0.93	1.01
Amos [3]	WC1	41	420	68	431	0.60	0.97
	WC2	46	310	47	363	0.98	0.85
	WC7	71	534	76	490	0.93	1.09
Liu and Soon [43]	P1NA	22	111	21	120	1.05	0.93
	F1NA	23	157	27	169	0.85	0.93
	P3NA	25	94	22	100	1.14	0.94
	F3NA	26	132	31	130	0.84	1.02
Avg						0.91	0.99
C.O.V (%)						14	7
		Overall					
Avg						0.94	0.99
C.O.V (%)						13	7

all specimens considered. Fig. 5 compares the experimental and numerical load vs. lateral displacement curves for infilled frames subjected to combined loading (specimen CF1-3) as well as subjected to lateral loading (specimen WB2) only. Both the table and figure show that the model is accurate in simulating behavior of an infilled steel frame under different levels of vertical load or without vertical load. Given that specimens were from different studies, this shows that the finite element model is robust for different material and geometric properties of infilled frames. Hence, the modeling technique used in this study was deemed valid and effective and was then used in the subsequent parametric study. From the point of view of experimental results, the combined loading study [42] shows that the presence of axial load resulted in an increase in both the lateral stiffness and strength of the infilled frame and the higher the axial load, the greater the increase. However, the available data points were not sufficient to define the exact correlation.

4. Parametric study

For the standard model, the bounding frame was made of W250 × 58 columns and W200 × 46 beams. The infill was 2800 mm high by 2800 mm long. The infill compressive strength, f'_m, was assumed to be 25 MPa and the tensile strength was taken as the 1/10th of f'_m. The elastic modulus of masonry, E_m, was determined as $850f'_m$ in accordance with CSA S304-14 [48]. The parameters considered included the magnitude of vertical loading and the manner of its application; infill aspect ratio; infill compressive strength; and bounding frame stiffness. The constitutive models, boundary conditions, and analysis procedure described in Section 3 are used in this parametric study.

Table 3 summarizes the finite element models used in this study. Five vertical load levels, V, representing 10%, 20%, 30%, 40%, and 50% of the axial capacity of 350W W250 × 58 [44] columns were studied. It is recognized that in practice, the vertical load may be applied directly through frame columns or some of it may be applied through the frame beam. Thus, for each vertical load level, three different manners of application were considered including: (1) applied as a uniformly distributed load (UDL) on the top beam of the frame; (2) applied as point loads at the top of two columns; and (3) half of the vertical load applied as UDL on the top beam and the other half as point loads at the top of two columns, referred to as 50–50 manner. Also included in the parametric studies were four aspect ratios of the infill (H/L = 0.78, 1.00, 1.40, 2.33)

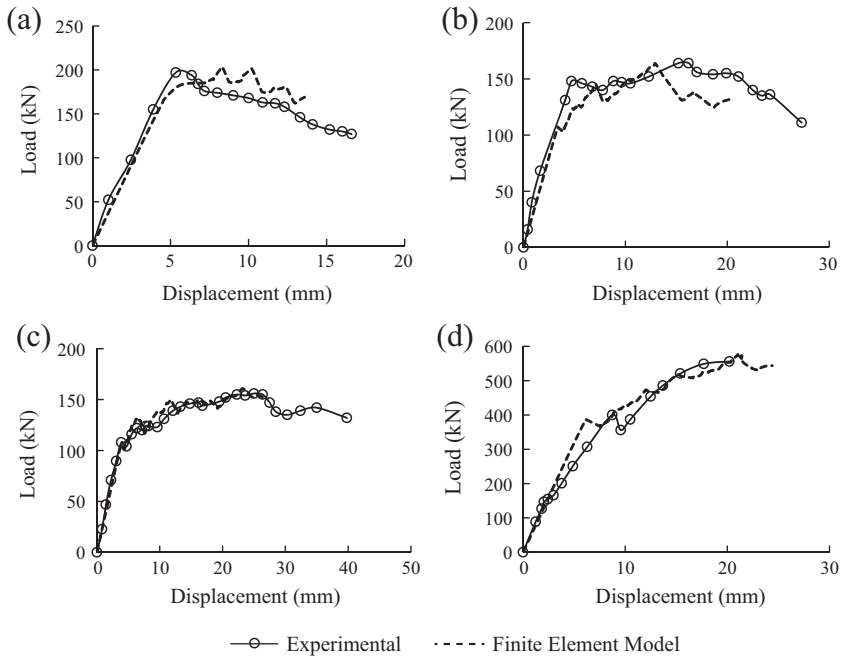

Fig. 5. Comparison of FE and experimental load vs. lateral displacement curves: (a) CF-1 [42]; (b) CF-2 [42]; (c) CF-3 [42]; and (d) WB2 [2].

Table 3
Summary of finite element models in the numerical study.

No. of models	Vertical load level (%)	H (m)	L (m)	Aspect ratio	f'_m (MPa)	Appl. method	Frame type	λL	p
24	0–50	2.8	1.2–3.6	0.78–2.33	25	UDL	Stand.	2.66–8.58	0–0.37
24	0–50	2.8	1.2–3.6	0.78–2.33	25	Point load	Stand.	2.66–8.58	0–0.37
24	0–50	2.8	1.2–3.6	0.78–2.33	25	50-50	Stand.	2.66–8.58	0–0.37
10	0–40	2.8	2–2.8	1.00–1.40	15	UDL	Stand.	4.17–5.92	0–0.29
6	0–50	2.8	3.6	0.78	15	UDL	Stand.	7.55	0–0.30
5	0–40	2.8	2.8	1	10	UDL	Stand.	5.35	0–0.30
18	0–50	2.8	2–3.6	0.78–2.33	25	UDL	Strong	3.19–5.78	0–0.19
18	0–50	2.8	2–3.6	0.78–2.33	25	UDL	Weak	5.70–10.32	0–0.37

covering a range of stocky to slender infills; three masonry compressive strengths (f'_m = 10, 15 and 25 MPa); and in addition to the standard model, a strong frame (W310 × 129 columns and W360 × 79 beam) and a weak frame (W150 × 24 columns and W100 × 19 beam). Columns of the strong and weak frame have an EI/L approximately 5 and 0.5 times respectively those of the standard model frame.

5. Discussion of results

5.1. Effect of vertical load level, V

In this case, the material and geometric properties of the standard model was used and the vertical load was assumed to be applied as a UDL on the frame beam. Please note that in this as well as the following sections, unless otherwise stated, the term "stiffness" refers to the cracking stiffness which was defined as the secant stiffness at the load corresponding to the first major diagonal crack, immediately after which a marked load drop occurred on the response curve. The crack stiffness rather than initial stiffness was selected because previous studies ([8,21]) suggested that the initial stiffness had more scatter due to the initial "engaging" stage of the infill and the frame and does not accurately represent the system stiffness once they behave together. The crack stiffness was a more reliable indicator of the system stiffness. In most cases, the load vs. displacement response remains linear up to the first major cracking load.

The finite element results showed that the effect of the vertical load level on the lateral stiffness and strength of the infilled system was also dependent on the aspect ratio of the infill. This collective effect can be seen in Fig. 6 where the applied vertical load V versus normalized cracking stiffness and ultimate load are plotted. The stiffness and ultimate load values are normalized with respect to the model of each aspect ratio but without vertical load. Fig. 6 shows that the presence of vertical load affects both the stiffness and strength of infilled systems to various degrees depending on infill aspect ratios. Overall, there seems to exist an optimal vertical load level up to which an increase in the vertical load results in an increase in both stiffness and strength of the system. A further increase above this level, however, the stiffness and strength begin to decrease gradually. This optimal load level varies for different infill aspect ratio and this is discussed in more detail in the next section.

The increase in stiffness and strength due to the presence of vertical load is believed to be attributed to the increase in diagonal strut width caused by the vertical load. This is qualitatively shown in Fig. 7. The strut width of the infill without vertical loading (Fig. 7 (a.i)) is much narrower than that of the infill with vertical load (Fig. 7(b.i)) during the loading. For the latter case, even after localized corner crushing of infill, there is still relatively large region in contact between the beam and infill at failure (Fig. 7(b.ii), which enables the more possible loading paths for lateral load transfer

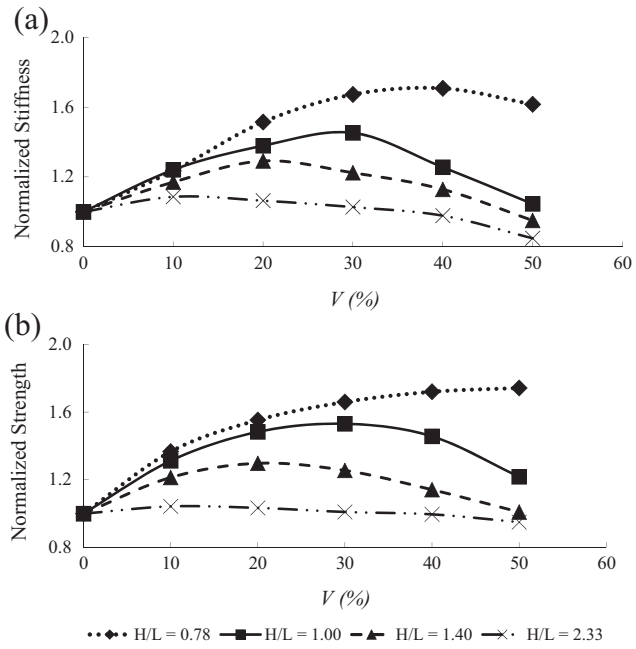

Fig. 6. Effect of vertical load level on (a) cracking stiffness and (b) strength of the infilled frame for varying infill aspect ratios.

thus achieving a higher ultimate load. However, as the vertical load increases, the local crushing at loaded corners occurs increasingly earlier. It is reasonable to deduce that at some vertical load level, the occurrence of crushing will outweigh the increase in the contact length. This is believed to be the reason that lateral strength of the infilled frame begin to decrease beyond the optimal load level.

5.2. Effect of aspect ratio, H/L

Referring to Fig. 6, it can be observed that the percentage increase in stiffness and strength caused by vertical load is increasingly significant as the infill becomes stockier. The behavior of the most slender infill ($H/L = 2.33$) seems to be least affected by the presences of vertical load. Shown in Fig. 8 is a plot of optimal vertical load level versus infill aspect ratio. It shows that in general, an increase in slenderness of the infill, corresponds to a decrease in the optimal load level. The lateral loading transfer mechanism for infills consists of flexure characterized by the overall bending of the infill and shear characterized by the diagonal strut action. It is reasonable to assume that more forces are transferred through flexural behavior than the diagonal strut action as infills become more slender. The benefit of vertical load on increasing the lateral strength by increasing the width of the diagonal strut is thus not significant for slender infills. On the other hand, the combined lateral and vertical loading results in second-order effects by magni-

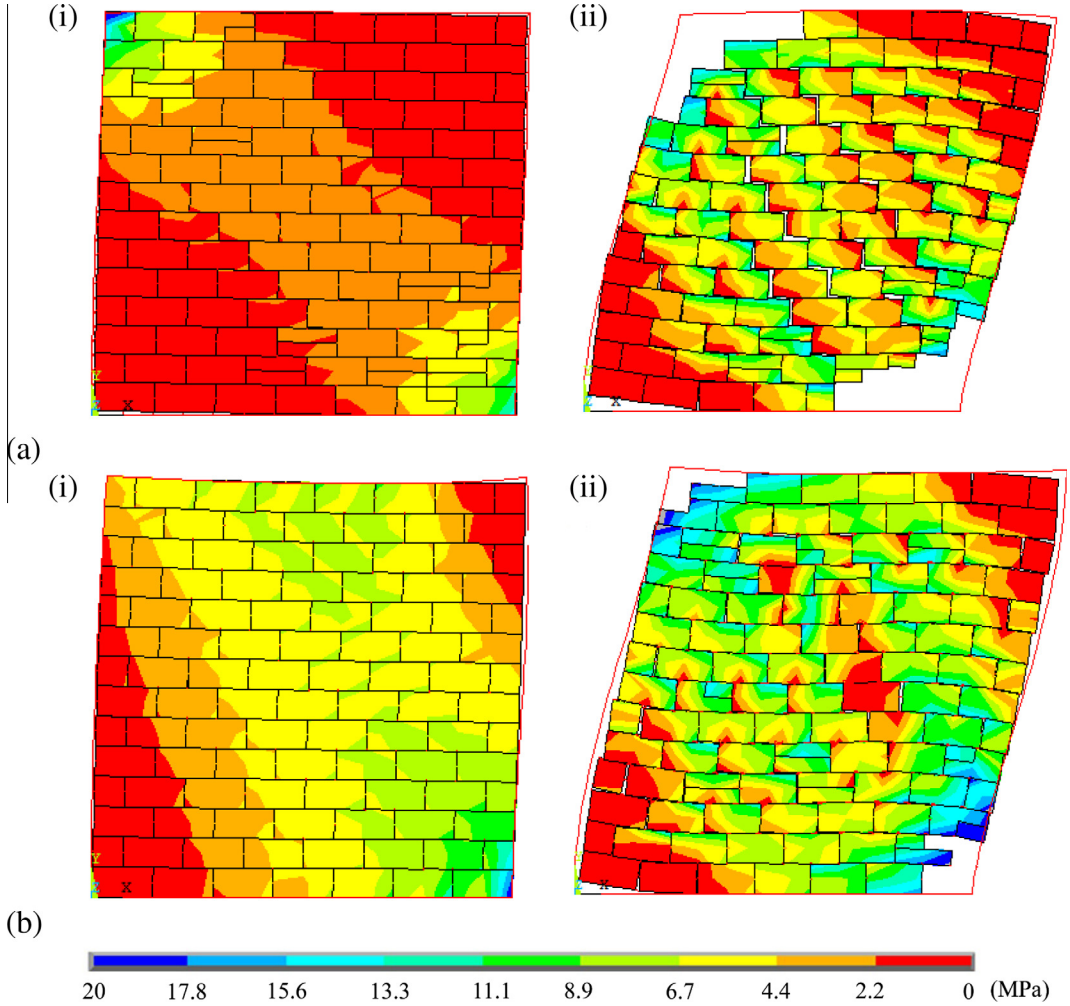

Fig. 7. FE distribution of compressive stress in the infill (a) subjected to only lateral load,; (b) subject to combined loading: (i) early stage of loading, (ii) at failure.

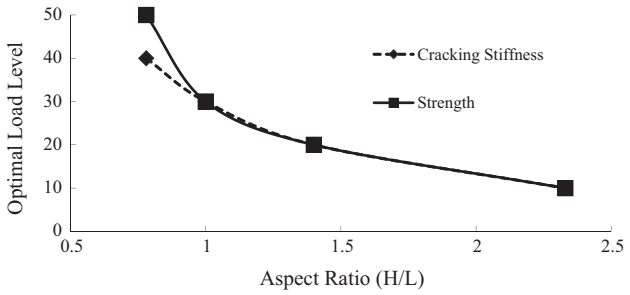

Fig. 8. Optimal load level vs aspect ratio for (a) cracking stiffness, and (b) strength.

fying the bending moment the infill experiences. This secondary effect is more pronounced for the slender infill than for the stocky infill. These two factors in combination attributed to the decrease of optimal load level as the aspect ratio of the infill increases.

5.3. Effect of infill compressive strength

The effect of varying masonry compressive strengths on infilled frames subjected to combined loading is presented in Fig. 9 for infill with an aspect ratio of 1.0 as an example. A similar trend was observed for other aspect ratios. The figure shows that the presence of vertical load on increasing the lateral stiffness and strength up to a certain level is true for all masonry compressive strengths studied. However, the optimal vertical load levels decrease as the compressive strength of infills decreases, from 30% for f'_m = 25 MPa to about 10% for f'_m = 10 MPa. At 40% vertical load level, infill failed directly by crushing even without any lateral load since the vertical load at this level is greater than (1.1 times) the compressive capacity of the infill. It is hence concluded that the benefit of vertical load is better realized for strong infills than for weak infills.

5.4. Effect of frame stiffness

The effect of frame stiffness on infilled frames subjected to combined loading is presented in Fig. 10 for the infill with an aspect ratio of 1.0 as an example. A similar trend was observed for other aspect ratios. As shown in the figure, the stiffness of the frame does influence the optimal load level and degree of stiffness and strength increase of the frame system due to the vertical load. As the frame stiffness increases, the optimal load level increases while the percentage increase due to vertical load decreases. This suggests that strong frames can sustain a higher level of vertical load up to which the increase in lateral stiffness and strength exists, however, the rate of this increase is less than the weak frame. For a given infill, at a same applied vertical load level, less vertical load is transferred to the infill in a strong frame than in a weak frame. Thus a strong frame can sustain a higher applied vertical load prior to the infill failure. However, the strong frame experiences less deformation due to its high rigidity and thus less increase in contact length than a relatively weak frame. This results in its lower rate of increase in stiffness and strength as the vertical load increases than weak frames.

5.5. Effect of vertical load application methods

Fig. 11 shows the effect of vertical load application methods for infills using aspect ratio of 1.0 as an example. The manner of vertical load application significantly affects the behavior of the infilled system especially between the cases of applying through the frame beam and through the frame columns. When the vertical load is applied through columns, the stiffness of infilled system shows a continuous increase trend as the vertical load level

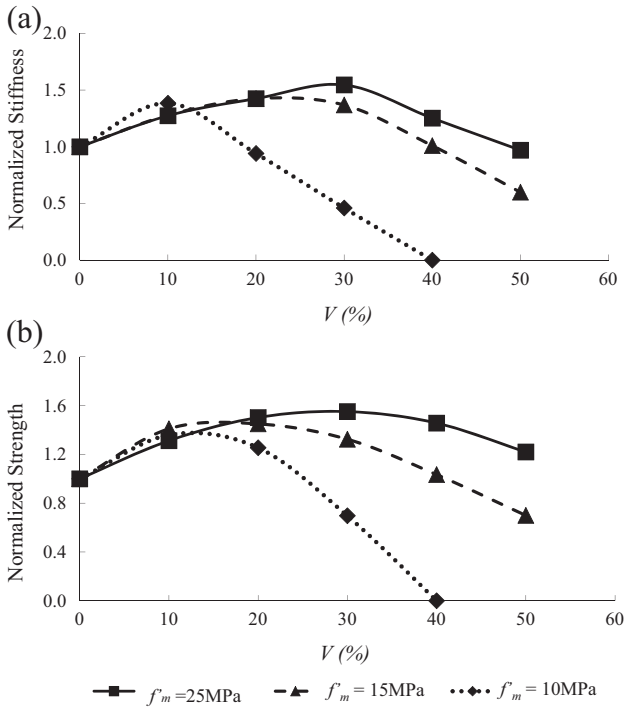

Fig. 9. Effect of masonry compressive strength on (a) cracking stiffness, and (b) strength of the infilled frame.

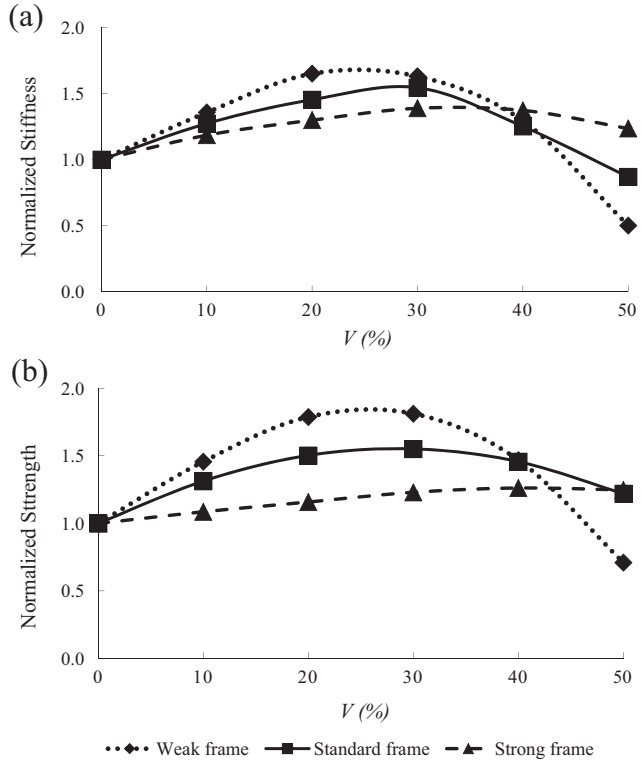

Fig. 10. Effect of frame stiffness on (a) cracking stiffness and (b) strength of the infilled frame.

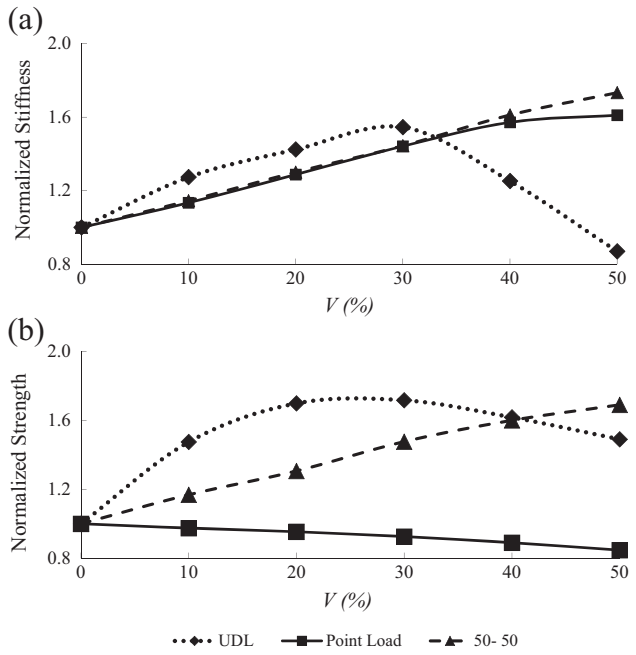

Fig. 11. Effect of vertical loading application methods on (a) cracking stiffness, and (b) strength of the infilled frame.

increases while the lateral strength of the infilled system showed an approximately linear decrease. When the vertical load is applied in the 50–50 manner, both the stiffness and strength seem to increase in a linear relationship with the increase in vertical load. This suggests that the benefit of vertical load applied through the beam outweighs the detrimental effect of vertical load applied through columns, resulting in a net result of beneficial effect on the lateral stiffness and strength of the infill.

The difference in behavior due to the manner of vertical load application is believed to be attributed to the load sharing between the infill and the frame. Table 4 lists the loads transferred through two columns, V_c, and the ratio of this load to the total applied vertical load, V for the case of V equal to the 10% of axial capacity of columns. The table shows that the columns experience significantly different amount of load among the three application methods. When the vertical load is applied as a UDL on the frame beam, the amount of load transferred through columns depends on the infill aspect ratio and more load is transferred to infills as the aspect ratio increases. The load transferred to infill will effectively increase the contact regions between the beam and the infill. When the vertical load is applied through columns, the majority of this load is directly transferred into columns (about 83%) which leaves a small portion (about 17%) transferred through infills. Thus the contact regions developed between the beam and infill are less than the former case. Instead, the shortening of columns makes loaded corner highly stressed. The already stressed corner crushes much earlier and more extensively as lateral load is applied than the case when no vertical load is present. This is believed to attribute to the negative impact on the lateral strength caused by vertical load applied directly through columns. It is important to note that this observation is different from that for RC frames where vertical load applied on columns was shown to increase the strength of the infilled frame. For RC frames, vertical load applied through columns delays cracking and thus results in increases in stiffness and ultimately the moment capacity of the columns. For steel columns, these beneficial effects of vertical load do not exist. Instead, the vertical load through columns reduces their moment capacity.

Table 4
Vertical load transferred through columns for different load application methods (V = 10% of axial capacity of column W250 × 28).

Aspect ratio	UDL		Point load		50–50	
	V_c (kN)	V_c/V (%)	V_c (kN)	V_c/V (%)	V_c (kN)	V_c/V (%)
2.33	331.4	63.8	447.6	86.2	395.6	76.2
1.40	209.6	40.4	434.0	83.6	337.4	65.0
1.00	150.4	28.9	430.4	82.9	307.0	59.1
0.78	117.4	22.6	430.0	82.8	288.4	55.5

6. Analytical model

6.1. Development of modification factor M_F

Based on the diagonal strut approach, the effect of vertical loading on the lateral stiffness and strength of the infilled frame may be considered through a modification factor M_F to the stiffness and strength of the infill subjected to lateral load only. Note that the "stiffness" used in this section also refers to the cracking stiffness as defined in Section 5. Due to the complexity of the problem, this study focused on vertical load applied as a UDL to the frame beam. To develop an analytical model that incorporates effects of aforementioned factors and also is simple to use, this study adopted the use of the unit-less factor λL to account for effects of both infill aspect ratio and relative infill and frame stiffness, and proposed the use of a vertical load ratio p as a measurement of vertical load level. Term λ was commonly used in previous studies [14–19] and can be defined as:

$$\lambda = \sqrt[4]{\frac{E_m t \sin(2\theta)}{4E_f I_c H}} \tag{5}$$

where E_m and E_f are the elastic moduli of masonry and the frame respectively; t, H and L are the thickness, height, and length of infill, respectively; I_c is the moment of inertia of the column, and $\theta = \tan^{-1}(H/L)$. The ratio p is defined as the applied vertical load divided by the combined axial capacity of columns and infill and can be expressed as:

$$p = \frac{V}{f'_m tL + 2A_c f_y} \tag{6}$$

where V is the applied vertical load, f'_m is the infill strength, A_c is the column cross-sectional area, and f_y is the yield strength of steel columns. The resulted λL and p values for all model specimens ranged from around 3 to 10.5 and 0 to 0.37 respectively as summarized in Table 3.

This study proposes that the modification factor M_F be expressed as follows where $f(p)$ and $g(\lambda L)$ are two independent functions:

$$M_F = 1 + f(p)g(\lambda L) \tag{7}$$

Fig. 12 plots the relationship between p and normalized stiffness and strength of infilled model specimens. For clarity, three λL scenarios are shown in the figure. The details of each scenario are described as follows: (1) λL = 2.66 corresponds to an infill with an aspect ratio of 2.33 and f'_m = 25 MPa and bounded by the standard frame; (2) λL = 4.53 corresponds to an infill with an aspect ratio of 1.00 and f'_m = 25 MPa and bounded by the strong frame; (3) λL = 7.55 corresponds to an infill with an aspect ratio of 0.78 and f'_m = 15 MPa and bounded by the standard frame. These three scenarios cover different combinations of infill aspect ratio, f'_m and frame stiffness therefore were chosen as examples for demonstration. Fig. 12 shows that the relationship between p and the increase in stiffness and strength is approximately parabolic. This observation is also true for other λL values in this study. Fig. 13 plots the λL

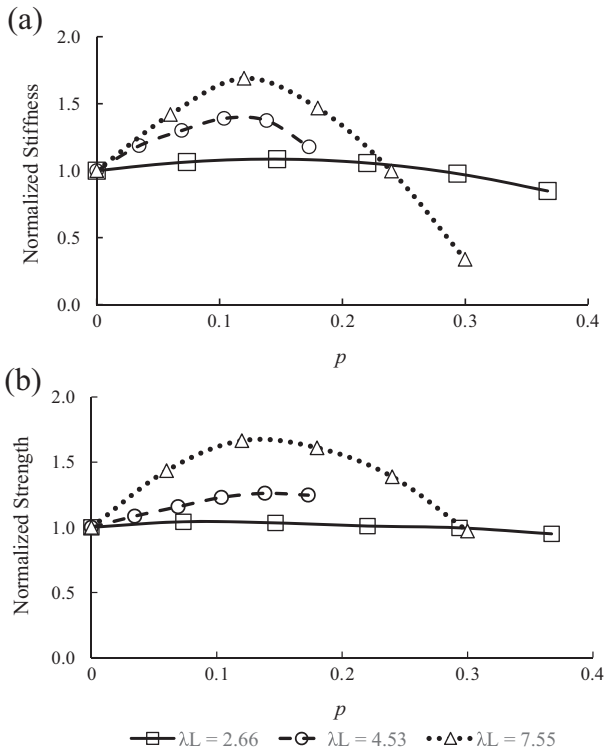

Fig. 12. Vertical load ratio p vs (a) normalized stiffness and (b) normalized strength.

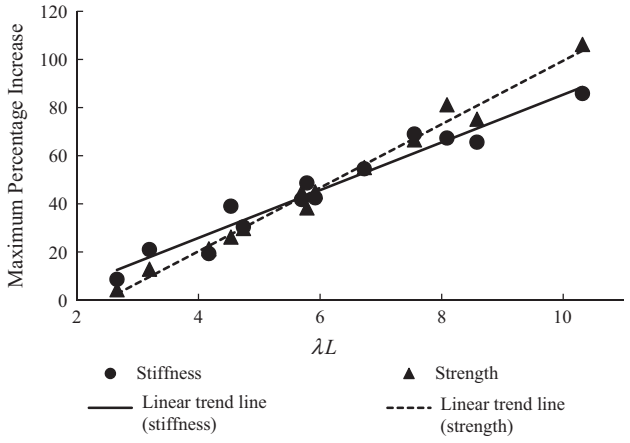

Fig. 13. λL vs maximum increase in stiffness and strength.

values vs. maximum increase of normalized stiffness and strength of infilled frames as a result of the vertical load increase. It can be seen that the maximum increase in both the stiffness and strength has an approximately linear relationship with λL values.

6.2. Equation of M_F and comparison with FE results

Based on the above discussion and through nonlinear regression analysis on results of finite element models, the expressions of $f(p)$ and $g(\lambda L)$ are then determined as follows:

For stiffness:

$$f(p) = -0.234p^2 + 0.594p \quad (8)$$

$$g(\lambda L) = 0.281\lambda L - 0.550\lambda L \quad (9)$$

For strength:

$$f(p) = -0.189p^2 + 0.560p \quad (10)$$

$$g(\lambda L) = 0.312\lambda L - 0.782\lambda L \quad (11)$$

The comparison of these sets of equations with FE results is illustrated in Fig. 14 where three scenarios of λL are illustrated. It can be seen that the proposed analytical equations achieve a good agreement with FE results. When FE results were compared with the equation values for all models, the stiffness Eqs. (8) and (9) obtained a $R^2 = 0.954$ while the strength Eqs. (10) and (11) obtained a $R^2 = 0.978$, indicating a good performance of analytical model over a wide range of parameters. It is noted though that the failure mode of all FE models was by corner crushing and hence Eqs. (10) and (11) should be used corresponding to this failure mode.

6.3. Application of M_F and limitations

The modification factor, developed based on normalized stiffness and strength trend as described above, is intended to be used to modify the stiffness and strength of the infills subjected to lateral load only. It is noted though that this modification factor equation was developed for infills bounded by steel frames with vertical load applied through frame beams. For other bounding frame material or vertical load applied in different manners, this set of equations is not directly applicable. Although the loading consid-

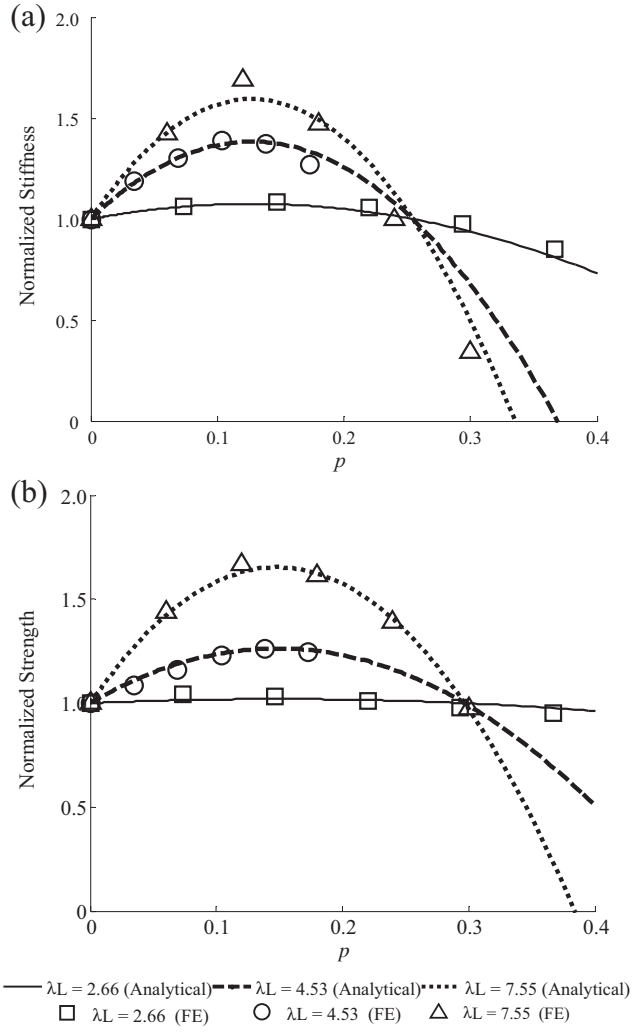

Fig. 14. Analytical model values vs. FE results: (a) stiffness and (b) strength.

ered was static, it is believed that the behavior trend and effects of parameters discussed are still valid for seismic loading situation. However, the analytical equations proposed should be thoroughly validated with results from seismic tests of infilled frames. Since the model used a single frame configuration with no openings in the infill, its applicability to multi-storey, multi-bay infilled frames and infills with openings needs further investigation.

7. Conclusions

A finite element model was developed to study the in-plane stiffness and strength of masonry infills bounded by steel frames subjected to combined lateral and vertical loading. A parametric study on the effect of vertical load levels, loading methods, infill aspect ratio and strength, and frame stiffness on the lateral stiffness and strength of infilled frames was conducted. A set of analytical equations was proposed to account for these parameters in the determination of infilled system stiffness and strength under combined loading. Some conclusions stemmed from this study are as follows:

When applied as a UDL on the frame beam, the presence of vertical load, up to a certain level, results in an increase in the lateral stiffness and strength of the infilled system. And beyond that level, the benefit of vertical load begins to diminish. This load level is defined as the optimal level. The optimal load level is found to be dependent on the infill aspect ratio, infill strength, and the bounding frame stiffness.

When the vertical load is applied on columns, the lateral stiffness of infilled system is increased with an increase in the vertical load level. However, the lateral strength shows a decrease. When the vertical load is applied in a 50–50 manner on both the frame beam and columns, infilled systems show almost linearly increasing stiffness and strength as the load level increases.

A set of equations for calculating modification factor M_F for vertical load effect is proposed for vertical load applied to the frame beam case. The equations are shown to produce results in good agreement with FE values for a wide range of vertical load levels. The development of M_F also considered the effect of aspect ratio and material strength of infills as well as frame stiffness.

Acknowledgements

The authors wish to recognize the contribution of financial assistance by the Canadian Concrete Masonry Producers Association and Natural Sciences and Engineering Research Council of Canada.

References

[1] McBride R. The behaviour of masonry infilled steel frames subjected to racking. MScE Thesis. New Brunswick, Canada: University of New Brunswick; 1984.
[2] Yong TC. Shear strength of masonry infilled panels in steel frames. MScE Thesis. New Brunswick, Canada: University of New Brunswick; 1984.
[3] Amos K. The shear strength of masonry infilled steel frames. MScE Thesis. New Brunswick, Canada: University of New Brunswick; 1985.
[4] Dawe JL, Seah CK. Behaviour of masonry infilled steel frames. Can J Civ Eng 1989;16(6):865–76.
[5] Henderson RC. Experimental and analytical investigation of out-of-plane and in-plane seismic drift in un-reinforced masonry infilled frames. PhD Dissertation. Knoxville: the University of Tennessee; 1994.
[6] Flanagan RD. Behavior of structural clay tile infilled frames. PhD Dissertation. Knoxville: The University of Tennessee; 1994.
[7] Al-Chaar G. Non-ductile behaviour of reinforced concrete frames with masonry infill panels subjected to in-plane loading. USACERL Technical Manuscript 99/18, US Army Corps of Engineers, Construction Engineering Research Laboratory. Champaign, Illinois; 1998.
[8] Liu Y, Soon S. Experimental study of concrete masonry infills bounded by steel frames. Can J Civ Eng 2012;39(2):180–90.
[9] Mehrabi AB, Shing PB. Finite element modeling of masonry-infilled RC frames. ASCE J Struct Eng 1997;123(5):604–13.
[10] Dawe JL, Seah CK, Liu Y. A computer model for predicting infilled frame behaviour. Can J Civ Eng 2001;28:133–48.
[11] El-Dakhakhni WW. Nonlinear finite-element modelling of concrete masonry-infilled steel frame. MScE thesis. Philadelphia: Drexel University; 2002.
[12] Stavridis A, Shing PB. Finite-element modeling of nonlinear behavior of masonry-infilled RC frames. J Struct Eng ASCE 2010;136(3):285–96.
[13] Mohyeddin A, Goldsworthy HM, Gad EF. FE modelling of RC frames with masonry infill panels under in-plane and out-of-plane loading. Eng Struct 2013;51:73–87.
[14] Gambarotta G, Lagomarsino S. Damage models for the seismic response of brick masonry shear walls. Part I: the mortar joint model and its applications. Earthq Eng Struct Dyn 1997;26:423–39.
[15] Gambarotta G, Lagomarsino S. Damage models for the seismic response of brick masonry shear walls. Part II: the continuum model and its application. Earthq Eng Struct Dyn 1997;26:441–62.
[16] Stafford-Smith B, Carter C. A method for the analysis of infilled frames. Proc Inst Civ Eng 1969;44:31–48.
[17] Mainstone R. On the stiffnesses and strengths of infilled frames. Proc Inst Civ Eng 1971(Supplement IV):57–90.
[18] Wood RH. Plasticity, composite action and collapse design of unreinforced shear wall panels in frames. Proc Instit Civ Eng 1978;65:381–411.
[19] Liauw TC, Kwan KH. Plastic theory of non-integral infilled frames. Proc Instit Civ Eng 1983;75(3):379–96.
[20] Flanagan RD, Bennett RM. In-plane behavior of structural clay tile infilled frames. J Struct Eng 1999;125(6):590–9. ASCE.
[21] Tucker CJ. Predicting the in-plane capacity of masonry infilled frames. Ph.D Thesis. Tennessee: Tennessee Technological University; 2007.
[22] Thiruvengadam V. On the natural frequencies of infilled frames. Earthq Eng Struct Dyn 1985;13(3):401–19.
[23] Chrysostomou CZ. Effects of degrading infill walls on the nonlinear seismic response of two-dimensional steel frames. Ph.D. thesis. Ithaca, NY: Cornell Univ.; 1991.
[24] Hamburger RO, Chakradeo AS. Methodology for seismic-capacity evaluation of steel-frame buildings with infill unreinforced masonry. Proc., National Earthquake Conf., vol. 2. Memphis, TN: Central U.S. Earthquake Consortium; 1993. p. 173–91.
[25] Crisafulli FG. Seismic behaviour of reinforced concrete structures with masonry infills. Ph.D. thesis. Christchurch, New Zealand: Univ. of Canterbury; 1997.
[26] Chrysostomou CZ, Gergely P, Abel JF. A six-strut model for nonlinear dynamic analysis of steel infilled frames. Int J Struct Stab Dyn 2002;2(3):335–53.
[27] El-Dakhakhni WW, Elgaaly M, Hamid AA. Three-strut model for concrete masonry-infilled steel frames. J Struct Eng 2003;129(2):177–85.
[28] Al-Chaar B, Mehrabi A. Constitutive models for nonlinear finite element analysis of masonry prisms and infill walls, Report ERDC/CERL TR-08-19. US Army Corps of Engineers; 2008.
[29] Lotfi HR, Shing PB. An appraisal of smeared crack models for masonry shear wall analysis. Comput Struct 1991;41(3):413–25.
[30] Mehrabi AB, Shing PB, Schuller MP, Noland JL. Experimental evaluation of masonry-infilled RC frames. J Struct Eng 1996;122(3):228–37.
[31] Stavridis Andreas, Analytical and experimental study of seismic performance of reinforced concrete frames infilled with masonry walls. Ph.D. Dissertation. San Diego, La Jolla, CA: University of California; 2010.
[32] Lotfi HR, Shing PB. An interface model applied to fracture of masonry structures. J Struct Eng, ASCE 1994;120(1):63–80.
[33] Fiorato AE, Sozen MA, Gamble WL. An investigation of the interaction of reinforced concrete frames with masonry filler walls. Technical Report No. UILU-ENG 70-100. Urbana-Champaign, Illinois: University of Illinois; 1970.
[34] Manos GC, Soulis VJ, Thauampteh J. The behavior of masonry assemblages and masonry-infilled R/C frames subjected to combined vertical and cyclic horizontal seismic-type loading. Adv Eng Softw 2012;45:213–31.
[35] Stylianidis KC. Experimental investigation of masonry unfilled R/C frames. Open Constr Build Technol J 2012;6(Suppl 1–M13):194–212.
[36] Papia M, Cavaleri L, Fossetti M. Infilled frames: developments in the evaluation of the stiffening effect of infills. Struct Eng Mech 2003;16(6):675–93.
[37] Cavaleri L, Fossetti M, Papia M. Effect of vertical loads on lateral response of infilled frames. In: Proceedings 13th world conference on earthquake engineering, Vancouver, Canada, No. 2931; 2004.
[38] Amato G, Cavaleri L, Fossetti M, Papia M. Infilled frames: influence of vertical load on the equivalent diagonal strut model. In: The 14th world conference on earthquake engineering. Beijing, China; 2008
[39] Campione G, Cavaleri L, Macaluso G, Amato G, Di Trapani F. Evaluation of infilled frames: an updated in-plane-stiffness macro-model considering the effects of vertical loads. Bull Earthq Eng 2015:2265–81. http://dx.doi.org/10.1007/s10518-014-9714-x. Online publication date: 1-Aug-2015.
[40] Asteris PG, Cavaleri L, Di Trapani F, Sarhosis V. A macro-modelling approach for the analysis of infilled frame structures considering the effects of openings and vertical loads. Struct Infrastruct Eng 2015:1–16. http://dx.doi.org/10.1080/15732479.2015.1030761.
[41] Stafford-Smith B. Model tests results of vertical and horizontal loading of infilled frames. Am Concr Instit, ACI J 1968;65(8):618–25.
[42] Liu Y, Manesh P. Concrete masonry infilled steel frames subjected to combined in-plane lateral and axial loading – an experimental study. Eng Struct 2013;52:331–9.
[43] Liu Y, Soon S. Experimental study of concrete masonry infills bounded by steel frames. Can J Civ Eng 2012;39(2):180–90.

[44] CAN/CSA S16-14. Design of steel structures. ON, Canada: Canadian Standard Association; 2014.
[45] Priestley MJN, Elder DM. Stress–strain curves for unconfined and confined concrete masonry. ACI J 1983;80(3):192–201.
[46] Lourenço PB, Rots JG. A solution for the macro-modelling of masonry structures. In: Proceedings of the 11th international brick/block masonry conference. Shanghai, China: Tongji University; 1997. p. 1239–49.
[47] Lourenço PB. Computational strategies for masonry structures. PhD thesis. Delft, Netherlands: Civil Engineering Department, Delft University of Technology; 1996.
[48] CAN/CSA S304.1-04. Design of masonry structures. ON, Canada: Canadian Standard Association; 2004.